Bistatic Forward-Looking SAR KDCT-FSFT-Based Refocusing Method for Ground Moving Target With Unknown Curve Motion

Zhutian Liu, *Student Member, IEEE*, Zhongyu Li, *Member, IEEE*, Chuan Huang, *Student Member, IEEE*, Junjie Wu, *Member, IEEE*, and Jianyu Yang, *Member, IEEE*

***Abstract*—In real application scenario of bistatic forward-looking synthetic aperture radar (BFSAR), ground moving target (GMT) is generally smeared severely in SAR image, due to its unknown range cell migration (RCM) and Doppler frequency migration (DFM). When GMT moves along an unknown curve trajectory, its high-order RCM and DFM (including the second- and third-order terms) would further aggravate the difficulty of GMT refocusing. To address this issue, an efficient GMT refocusing method via keystone-based delay-correlation transform and fast searching Fourier transform (KDCT-FSFT) is proposed. First, the KDCT is proposed to correct the first- to third-order RCMs regardless of target's motion state and position information. Meanwhile, the order of GMT's phase response is reduced as well. Then, FSFT is applied to estimate the third-order Doppler parameter of GMT. In the following, a 2-D fast Fourier transform (2D-FFT) can be applied to integrate the target signal coherently in Doppler parameters domain, where the Doppler centroid and Doppler frequency rate of GMT can be estimated. Finally, with the aforesaid estimated Doppler parameters, RCM and DFM can be well corrected and target with unknown curve motion can be finely refocused. Compared with the existing methods, not only the refocusing accuracy of the proposed method is higher, but also its processing is more efficient, since the procedures in the proposed method are performed with respect to all the range cells in the corresponding aperture, i.e., GMT refocusing is achieved by the 2-D data received in one aperture, rather than along every single range cell. Both the simulation and experimental results are given to validate the effectiveness of the proposed method.**

***Index Terms*—Bistatic forward-looking synthetic aperture radar (BFSAR), keystone-based delay-correlation transform (KDCT), fast searching Fourier transform (FSFT), ground moving target refocusing, parameter estimation.**

I. Introduction

In recent years, bistatic forward-looking synthetic aperture radar (BFSAR) is increasingly attractive in both civilian and military fields, because it can provide high-resolution day- and night-time images of the forward-looking terrain in flight direction with all-weather conditions [1]–[3]. Due to the physical separation of transmitter and receiver, BFSAR with a proper geometry can break through the limitations of monostatic SAR and exhibits advantages of high anti-interference and flexibilities. With these superiority and its unique forward-looking observation ability, BFSAR plays a crucial role in modern remote sensing applications, such as autonomous navigation, self-landing and etc [4]–[6].

With the development of the BFASR system, ground moving target (GMT) refocusing, tracking and identification are enormously demanded [7]–[16]. When a GMT is presented in the observation scenario, GMT signal is usually smeared into multiple cells, since its non-cooperative motion inevitably induces unknown range cell migration (RCM) and Doppler frequency migration (DFM). Additionally, if GMT moves along a curve trajectory, the defocused effect of the high-order RCM and DFM (including the second- and third-order terms) should be taken into consideration, especially for the BFSAR systems. Thus, to effectively refocus GMT, the RCM and DFM, including the high-order terms, caused by GMT's curve motion should be compensated first. As we know, if the Doppler parameters of GMT are accurately obtained, defocused effect can be well compensated and GMT can be well refocused at its actual location in image. Thus, estimating GMT's Doppler parameters is one effective way to solve the refocusing problem for GMT with unknown curve motion. However, if one wants to accurately estimate the Doppler parameters, the RCM has to be well corrected first, while if one wants to completely correct the RCM, the Doppler parameters has to be obtained first [17]. The coupling relationship between RCM correction (RCMC) and parameter estimation will further aggravate the difficulty to refocus a GMT with unknown curve motion.

However, the current literature and reports of BFSAR are mainly focused on stationary scenario imaging algorithms, such as range Doppler algorithms, chirp scaling algorithms, Omega-k algorithms and etc [18]–[21]. For the purpose of focusing GMT for bistatic SAR, a parameter estimation and imaging method in [22] is put forward based on range-compressed curve fitting and 1-D searching, but its performance will be severely affected by the signal to noise ratio (SNR) and the fitting error. Zhu *et al.*

Manuscript received May 26, 2020; revised July 21, 2020; accepted August 4, 2020. Date of publication August 14, 2020; date of current version August 31, 2020. This work was supported in part by the National Natural Science Foundation of China under Grant 61901088, Grant 61922023, Grant 61771113, and Grant 61801099, in part by the Postdoctoral Innovation Talent Support Program under Grant BX20180059, and in part by the China Postdoctoral Science Foundation under Grant 2019M65338 and Grant 2019TQ0052. *(Corresponding author: Zhongyu Li.)*

The authors are with the School of Information and Communication Engineering, University of Electronic Science and Technology of China, Chengdu 611731, China (e-mail: neroleo@163.com; zhongyu_li@hotmail.com; huangchuan@std.uestc.edu.cn; junjie_wu@uestc.edu.cn; jyyang@uestc.edu.cn).

Digital Object Identifier 10.1109/JSTARS.2020.3016696

[23] proposed the Radon-Wigner distribution (RWD) method to obtain the Doppler parameters for GMT imaging in bistatic SAR. However, RWD method only considers the first-order RCM and estimates the first- to second-order Doppler parameters. As a consequence, due to the effect of the high-order RCM and DFM mentioned above, GMT with a curve motion in BFSAR would still be defocused after performing RWD. To address these issues for BFSAR, Li *et al*. [24] proposed the first-order keystone transform (KT) [25], [26] and the extend azimuth nonlinear chirp scaling (NLCS) [27], [28] to correct the range walk and equalize the Doppler frequency rate (DFR) of stationary background, respectively. Then, a product second-order ambiguity function (PSAF) is designed for the moving target detection and DFR estimation. A moving target imaging and velocity estimation method based on mismatched compression is proposed in literature [29]. However, these two methods involves two drawbacks: 1) only working with a high SNR and 2) the effect of the third-order RCM and DFM are ignored, only the second-order phase model is considered. Thus, the above-mentioned methods are not suitable to refocus GMT with a curve motion in BFSAR. Furthermore, these methods are processed along every range cell, which would make refocusing processing inefficiency.

To solve the aforesaid problems, we develop a keystone-based delay correlation transform (KDCT) and fast searching Fourier transform (FSFT)-based refocusing method in BFSAR for GMT with unknown curve motion. This method proposes the KDCT, which is processed in range frequency-azimuth time domain for the echo during the aperture time, to effectively and simultaneously correct the first- to third-order RCMs of GMT without any priori motion information. With the proposed KDCT, not only RCM is corrected, but also the order of DFM is reduced as well. Then, in order to compensate the defocusing effect of the third-order Doppler parameter, FSFT is utilized for estimation of the third-order Doppler parameter. After phase compensation and performing 2D-fast Fourier transform (2D-FFT), GMT can be accumulated into a peak in Doppler centroid-Doppler frequency rate domain (DC-DFR), where the peak position accurately determines the first- and second-order parameters. Finally, RCM and DFM can be well corrected with the estimated parameters, and GMT with unknown curve motion can be finely refocused.

Compared with the existing methods, a better performance on refocusing GMT with unknown curve motion can be obtained, since the first- to third-order Doppler parameters can be estimated effectively. Meanwhile, the proposed method can be easily implemented by complex multiplications and FFTs, which decreases the computational complexity. Furthermore, the proposed GMT refocusing method are performed with respect to all the range cells in the corresponding aperture, instead of every range cell, which makes the proposed method more efficient.

The remainder of this article is organized as follows. Section II gives the signal model of GMT in BFSAR and echo property analysis. Section III introduces the principle of the proposed KDCT-FSFT-based refocusing method. The effectiveness of the proposed method is demonstrated by simulation and experimental results in Section IV and Section V. Finally, Section VI concludes this article.

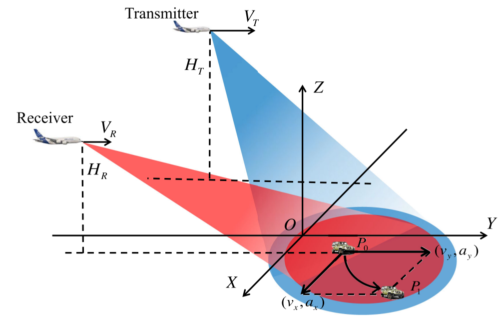

Fig. 1. The geometry configuration between BFSAR and GMT moving along a curve trajectory.

II. Signal Model and Echo Property Analysis

In this section, GMT signal model is constructed based on a general BFSAR geometry configuration. Meanwhile, the properties of RCM and DFM in BFSAR echo are analyzed in detail.

A. Signal Model

The geometry configuration between BFSAR platforms and a GMT with a curve motion is shown in Fig. 1. Receiver flies along the y-axis with the velocity V_R and Transmitter flies with V_T. The original coordinates of the receiver and transmitter are (X_R, Y_R, H_R) and (X_T, Y_T, H_T), respectively. The velocity vector of GMT is $(\vec{v}_t; \vec{a}_t) = (v_x, v_y; a_x, a_y)$, where v_x, a_x, v_y and a_y denote, respectively, the cross-track velocity, cross-track acceleration, along-track velocity and along-track acceleration. Assume that the point P_0 is the position of GMT at the beam center crossing time and it moves to $P_1(x_1, y_1)$ during the aperture time.

Supposing the transmitted signal is a linear frequency modulated (LFM) signal, BFSAR echo after demodulation can be expressed as

$$S(\tau, t) = rect\left(\frac{t}{T_a}\right) rect\left(\frac{\tau - \Delta\tau}{T_p}\right) \times \exp\left\{j\pi K_r (\tau - \Delta\tau)^2\right\} \exp\left\{-j2\pi f_c \Delta\tau\right\} \quad (1)$$

where τ is the fast time and t is the slow time. T_a, T_p, K_r, and f_c denote the aperture time, the pulse duration, the range frequency modulated rate and the carrier frequency, respectively. $\Delta\tau = R(t)/c$ denotes the delay time, c is the speed of light. $R(t)$ presents the instantaneous bistatic range and it can be given by

$$R(t) = R_R(t) + R_T(t) \quad (2)$$

where $R_R(t)$ and $R_T(t)$ are the slant range histories with respect to GMT of the receiver and the transmitter, respectively. $R_R(t)$

and $R_T(t)$ are given in (3) and (4), shown at the bottom of this page.

After range compression, the received signal of GMT in range frequency azimuth time domain can be expressed as

$$S(f_\tau,t)=rect\left(\frac{t}{Ta}\right)rect\left(\frac{f_\tau}{B_\tau}\right)\exp\left\{-j2\pi\frac{f_\tau+f_c}{c}R(t)\right\} \tag{5}$$

where f_τ is range frequency and B_τ is bandwidth.

Considering that GMT moves along an unknown curve trajectory, expanding $R_R(t)$ and $R_T(t)$ (jointly denoted as $R_{R,T}(t)$ for simplicity) at the beam center crossing time $t=0$ into Taylor series and keeping up to third-order terms yields, we have

$$R_{R,T}(t)\approx R_{R0,T0}+A_{R,T}t+\frac{1}{2}B_{R,T}t^2+\frac{1}{6}\mathrm{C}_{R,T}t^3 \tag{6}$$

where $A_{R,T}$, $B_{R,T}$ and $C_{R,T}$ are the first-, second- and third-order expanding coefficients of $R_{R,T}(t)$, respectively. These coefficients are given in (7), (8), and (9), shown at the bottom of this page. And $R_{R0,T0}$, $\cos\theta_{Rx,Tx}$ and $\cos\theta_{Ry,Ty}$ can be expressed as

$$\begin{aligned}R_{R0,T0}&=R_{R,T}(0)\\&=\sqrt{H_{r,t}^2+(X_{r,t}-x)^2+(Y_{r,t}-y)^2}\end{aligned} \tag{10}$$

$$\cos\theta_{Rx,Tx}=\frac{x-X_{r,t}}{R_{R0,T0}} \tag{11}$$

$$\cos\theta_{Ry,Ty}=\frac{y-Y_{r,t}}{R_{R0,T0}} \tag{12}$$

From the expressions (7)-(9), it can be found that the first-order expanding coefficient $A_{R,T}$ is related to the target along-track velocity v_y and cross-track velocity v_x. The second- and third-order coefficients are associated with the GMT velocity parameters (v_x,v_y,a_x,a_y).

For the convenience of analysis, set $R_0=R_{R0}+R_{T0}$. $\alpha=\mathrm{A}_R+\mathrm{A}_T$, $\beta=B_R+B_T$ and $\varepsilon=C_R+C_T$ are the first- to third-order Doppler parameter, respectively. Therefore, (5) can be rewritten as

$$\begin{aligned}S_1(f_\tau,t)=&\,rect\left(\frac{t}{Ta}\right)rect\left(\frac{f_\tau}{B_\tau}\right)\\&\times\exp\left\{-j2\pi\frac{f_\tau+f_c}{c}\left(R_0+\alpha\mathrm{t}+\frac{1}{2}\beta t^2+\frac{1}{6}\varepsilon t^3\right)\right\}\end{aligned} \tag{13}$$

The Doppler centroid f_{dc}, the Doppler frequency rate f_{dr} and the third-order Doppler frequency f_{d3} of GMT can be expressed as

$$f_{dc}=-\frac{\alpha}{\lambda}=-\frac{A_R+A_T}{\lambda} \tag{14}$$

$$f_{dr}=-\frac{\beta}{\lambda}=-\frac{B_R+B_T}{\lambda} \tag{15}$$

$$f_{d3}=-\frac{\varepsilon}{\lambda}=-\frac{C_R+C_T}{\lambda} \tag{16}$$

Thus far, the signal model of GMT in BFSAR has been constructed. In the following subsection, the echo properties of GMT in BFSAR are analyzed in detail.

B. Echo Property Analysis

In this subsection, the analysis of BFSAR echo property is based on the parameters of the typical applications given in Table I. Considering that the angle from GMT's motion direction to the positive $y-$axis is 45 degrees and the cross-track acceleration a_x is equal with the along-track acceleration a_y. In analyzing echo property, target with different cross- and

$$R_R(t)=\sqrt{H_r^2+\left(X_r-\left(x+v_xt+\frac{1}{2}a_xt^2\right)\right)^2+\left(Y_r+V_Rt-\left(y+v_yt+\frac{1}{2}a_yt^2\right)\right)^2} \tag{3}$$

$$R_T(t)=\sqrt{H_t^2+\left(X_t-\left(x+v_xt+\frac{1}{2}a_xt^2\right)\right)^2+\left(Y_t+V_Tt-\left(y+v_yt+\frac{1}{2}a_yt^2\right)\right)^2} \tag{4}$$

$$\mathrm{A}_{R,T}=\frac{v_x(x-X_{r,t})+(v_y-V_{R,T})(y-Y_{r,t})}{R_{R0,T0}}=v_x\cos\theta_{Rx,Tx}+(v_y-V_{R,T})\cos\theta_{Ry,Ty} \tag{7}$$

$$B_{R,T}=\frac{(V_{R,T}-v_y)^2\sin^2\theta_{Ry,Ty}+v_x^2\sin^2\theta_{Rx,Tx}+2v_x(V_{R,T}-v_y)\cos\theta_{Rx,Tx}\cos\theta_{Ry,Ty}}{R_{R0,T0}}+a_x\cos\theta_{Rx,Tx}+a_y\cos\theta_{Ry,Ty} \tag{8}$$

$$\begin{aligned}C_{R,T}=&\,3\frac{a_xv_x\sin^2\theta_{Rx,Tx}+a_y(v_y-V_{R,T})\sin^2\theta_{Ry,Ty}-a_x(v_y-V_{R,T})\cos\theta_{Rx,Tx}\cos\theta_{Ry,Ty}-a_yv_x\cos\theta_{Rx,Tx}\cos\theta_{Ry,Ty}}{R_{R0,T0}}\\&-\frac{3((V_{R,T}-v_y)^2+v_x^2)(v_x\cos\theta_{Rx,Tx}+(v_y-V_{R,T})\cos\theta_{Ry,Ty})}{R_{R0,T0}^2}+\frac{3((v_y-V_{R,T})\cos\theta_{Ry,Ty}+v_x\cos\theta_{Rx,Tx})^3}{R_{R0,T0}^2}\end{aligned} \tag{9}$$

TABLE I
SYSTEM PARAMETERS FOR ECHO PROPERTY ANALYSIS

Parameters	Values
Center frequency	$10GHz$
Range bandwidth	$300MHz$
Pulse repetition frequency	$1500Hz$
Platform velocity	$160m/s$
Transmitter's location	$(-800, -200, 1000)m$
Receiver's location	$(0, -600, 1200)m$

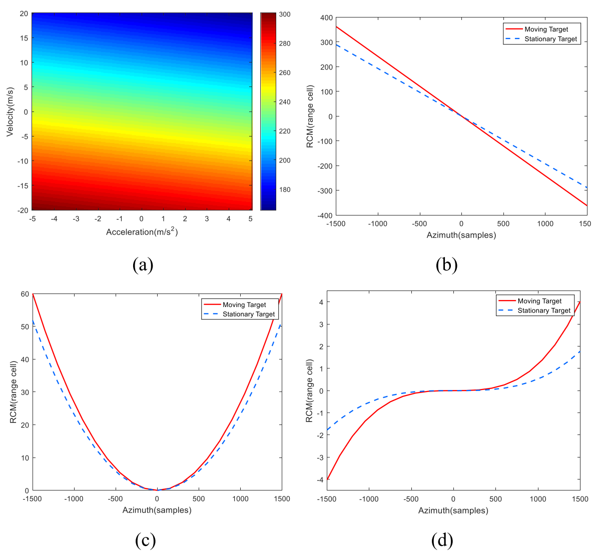

Fig. 2. RCM of GMT with an unknown curve motion. (a) RCM variation with velocities and accelerations. (b) Range walk. (c) Range curvature. (d) Third-order RCM.

along-track velocities (0–20 m/s) and accelerations (0–5 m/s^2) are considered.

From (13), RCM of the GMT with a curve motion in BFSAR can be expressed as

$$\begin{aligned} R_{rcm} &= \alpha t + \frac{1}{2}\beta t^2 + \frac{1}{6}\varepsilon t^3 \\ &= -\lambda\left(f_{dc}t + \frac{1}{2}f_{dr}t^2 + \frac{1}{6}f_{d3}t^3\right) \end{aligned} \tag{17}$$

Inspecting (17), the first term related to f_{dc} denotes range walk of GMT. The second term related to f_{dr} and the third term related to f_{d3} are range curvature and the third-order RCM, respectively. The analysis results of RCM are shown in Fig. 2. Fig. 2(a) shows that the maximum RCM variation of GMT in BFSAR with different velocities and accelerations within the synthetic aperture time. The color scale is in the number of the migrated range cells. It is clearly shown that the RCM of GMT is two-dimensionally varied along velocity $\vec{v}_t$ and acceleration $\vec{a}_t$. In addition, GMT signal will be dispersed into hundreds range cells as shown in Fig. 2(a).

In order to further analyze the property of RCM in BFSAR, a target with curve motion and a stationary target, which are located at the same position at the beam crossing time, are considered. Assuming that the velocity vector of GMT is set to be

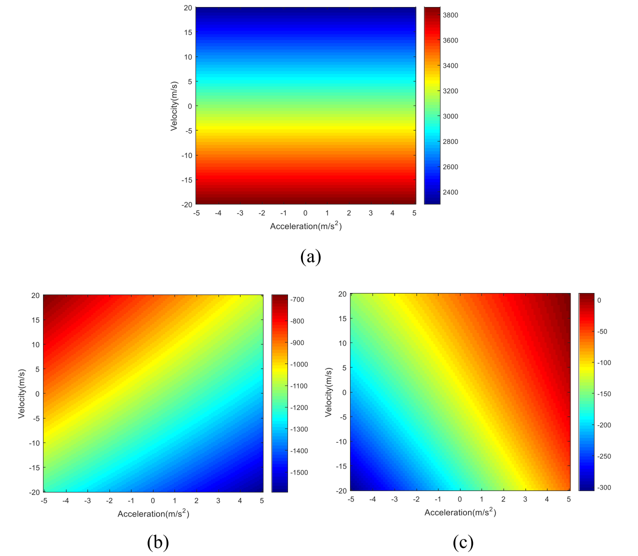

Fig. 3. Doppler frequency of GMT with an unknown curve motion. (a) Doppler centroid with velocities and accelerations. (b) Doppler frequency rate with velocities and accelerations. (c) Third-order Doppler frequency with velocities and accelerations.

$(-20$ m/s, -20 m/s; -3 m/s^2, -3 m/s$^2)$. The range walk, range curvature and the third-order RCM of these two targets are given in Fig. 2(b)–2(d). The red solid lines represent the corresponding RCMs of GMT and the blue dashed lines represent those of the stationary target. From Fig. 2(b)–2(d), we can observe that all the RCMs of GMT are larger than the stationary target, due to the additional curve movement. In Fig. 2(b), range walk is the major part of RCM in BFSAR, and the maximum range walk of GMT is about 360 range cells, which is 80 range cells more than that of the stationary target. Fig. 2(c) and Fig. 2(d) show that the maximum range curvature and third-order RCM of GMT are about 60 cells and 4 cells, respectively. Since range walk, range curvature and the third-order RCM of GMT with a curve motion are more than one range cell, thus the three kinds of RCMs cannot be ignored and should be compensated before GMT refocusing.

However, if the RCMs of GMT are compensated with the Doppler parameters of the stationary target, GMT signal cannot be gathered into one range cell and the residual RCM is about hundred range cells. As a consequence, the performance on GMT refocusing will be severely degraded. Therefore, for the purpose of complete RCMC for GMT, f_{dc}, f_{dr}, and f_{d3} of GMT should be estimated accurately.

Similarly, from (13), the azimuth phase of GMT with a curve motion can be expressed as

$$\begin{aligned} \varphi_{azi} &= -\frac{2\pi f_c}{c}\left(R_0 + \alpha t + \frac{1}{2}\beta t^2 + \frac{1}{6}\varepsilon t^3\right) \\ &= \pi\left(-\frac{2R_0}{\lambda} + 2f_{dc}t + f_{dr}t^2 + \frac{1}{3}f_{d3}t^3\right) \end{aligned} \tag{18}$$

In (18), it can be seen that the azimuth phase of GMT is contributed by f_{dc}, f_{dr}, and f_{d3}. With the system parameters in Table I, the variation of Doppler frequency with $(\vec{v}_t; \vec{a}_t)$ are shown in Fig. 3. Fig. 3(a) shows the maximum variation of f_{dc} related to α with different velocities and accelerations within the synthetic aperture time. The color scale is in Hz. We can observe that f_{dc} is only related to target velocity and the variation is one-dimensional. Note that f_{dc} of GMT is changed from 2300 to 3800 Hz, which is much larger than the pulse repetition frequency (PRF) of BFSAR system. As a result, GMT's Doppler spectrum may be splitting into two adjacent PRF bands. This phenomenon is called the Doppler centroid ambiguity, which would lead to the performance degradation of RCMC and GMT refocusing. Thus, the effect of the Doppler centroid ambiguity should be eliminated.

Fig. 3(b) and 3(c) are the maximum variation of f_{dr} related to β and f_{d3} related to ε with different velocities and accelerations within the synthetic aperture time. The color scales are in Hz/s and Hz/s^2, respectively. It can be seen form these two Figures that the variation trends of f_{dr} and f_{d3} are two-dimensional. The variation trend of f_{d3} and f_{dr} are more complicated than f_{dc}. In general, when phase error is less than $\pi/4$, the effect of the azimuth phase can be ignored for target refocusing [36]. According to the third term in (18), only when the absolute value of f_{dr} is less than 0.11 Hz/s, the azimuth phase related to f_{dr} is less than $\pi/4$. However, the variation range of f_{dr} in Fig. 3(b) is from -1600 Hz/s to -700 Hz/s. The boundary value is much greater than the conditional value and that is to say the second-order phase caused by f_{dr} cannot be ignored in target refocusing. Similarly, from Fig. 3(c), f_{d3} is varied from -300 Hz/s^2 to 10 Hz/s^2 and the maximum azimuth phase related to f_{d3} is changed from -100π to 3π with the different moving state of GMT. The variation range of the third-order phase caused by f_{d3} of the GMT with curve motion is far outweigh $\pi/4$. Thus, the effect of f_{d3} cannot be ignored as well. As a consequence, the second- and third-order azimuth phase should be taken into account in the following BFSAR GMT refocusing.

According to the echo property analysis, RCMs and the azimuth phase of GMT with a curve motion is strongly relevant to f_{dc}, f_{dr}, and f_{d3} in BFSAR cases. The effect of RCMs and azimuth phase related to f_{d3}, which are usually neglected in bistatic side-looking SAR, has to be eliminated. Thus, the third-order azimuth phase in (18) should be considered and the effect of f_{d3} cannot be ignored in BFSAR. In the succeeding section, the BFSAR KDCT-FSFT-based refocusing method is proposed for GMT with unknown curve motion.

III. Method Description

As mentioned in the previous analysis, the Doppler centroid f_{dc} of the received signal is large due to the receiver's forward-looking working mode. Usually, the large f_{dc} results in the Doppler centroid ambiguity. As a consequence, the GMT Doppler spectrum may be split into two adjacent PRF bands [24]. Thus, the Doppler centroid ambiguity should be suppressed first, and the pre-filtering function is constructed as

$$H_{pre} = \exp\left\{-j2\pi f_{ref}\frac{f_\tau + f_c}{f_c}t\right\} \tag{19}$$

where f_{ref} is the reference Doppler centroid.

And then, the pre-filtered GMT signal can be expressed as

$$\begin{aligned} S_2(f_\tau, t) &= rect\left(\frac{t}{Ta}\right) rect\left(\frac{f_\tau}{B_\tau}\right) \\ &\times \exp\left\{-j2\pi\frac{f_\tau + f_c}{c}\left(R_0 + \alpha' t + \frac{1}{2}\beta t^2 + \frac{1}{6}\varepsilon t^3\right)\right\} \end{aligned} \tag{20}$$

where $\alpha' = \alpha + \lambda f_{dcref}$ is the residual first-order coefficient of the instantaneous bistatic range $R(t)$. Comparing (13) and (20), we can find that the first-order coefficient has been decreased after the pre-filtering. Thus, a Doppler shift is introduced by the pre-filtering and the Doppler spectrum can be moved into one PRF band. Meanwhile, it is noteworthy that the first-order coupling relationship is lessened as well via the pre-filtering.

From GMT signal in (20), it can be seen that t-term, t^2-term and t^3-term are coupled with the range frequency f_τ, which correspond to range walk, range curvature and the third-order RCM, respectively. However, these three kinds of RCMs can not be well dealt with in a single processing step by the existing methods, such as KT [25], [26], Hough transform (HT) [30] and the second-order KT [31]. Symmetrical keystone transform (SKT) proposed in [32] is an effective way to compensate range walk and range curvature of GMT. However, by performing SKT, all the odd-order Doppler parameters of GMT are lost, which means that the first- and third-order Doppler parameters can't be estimated from the signal processed by SKT. As a result, GMT refocusing performance is deteriorated. Thus, to refocus a GMT moving along a curve trajectory, the RCMs have to be well corrected first and the Doppler parameters information should be retained in target signal.

Inspired by [33], [34], the KDCT is proposed to simultaneously correct the first- to third-order RCMs of GMT with a curve motion in this article. After pre-filtering, the KDCT is processed in range frequency-azimuth time domain and it can be expressed as

$$S_3(f_\tau, t) = S_2\left(f_\tau, \sqrt{\xi}\cdot t\right) S_2^*\left(f_\tau, \sqrt{\xi}\cdot (t - t_0)\right) \tag{21}$$

where ξ is the scale factor given by $f_c/(f_\tau + f_c)$. t_0 denotes the fixed delay given by $T_a/4$ [35].

Then, the transformed signal can be obtained as [37]

$$\begin{aligned} S_3(f_\tau, t) &\approx rect\left(\frac{t}{Ta}\right) rect\left(\frac{t - t_0}{Ta}\right) rect^2\left(\frac{f_\tau}{B_\tau}\right) \\ &\times \exp\left\{j\frac{2\pi}{\lambda}\left(-\alpha' t_0 + \frac{1}{2}\beta t_0^2 + \frac{1}{6}\varepsilon t_0^3\right)\right\} \\ &\times \exp\left\{-j2\pi F_2 t\right\} \exp\left\{-j2\pi F_1 f_\tau\right\} \\ &\times \exp\left\{-j\frac{\pi}{\lambda}\varepsilon t_0 t^2\right\} \end{aligned} \tag{22}$$

where $F_2 = (2\beta t_0 - \varepsilon t_0^2)/2\lambda$ is related to the Doppler frequency rate of GMT, and $F_1 = (6\alpha' t_0 + \varepsilon t_0^3)/12c$ is related to the Doppler centroid. The phase in the second and third exponential terms in (22) are the first-order term of slow-time t_m and range frequency f_τ, respectively, whose coefficients are related to GMT's Doppler parameters and the delay t_0 in azimuth. The last exponent is an additional modulation term introduced by GMT's third-order Doppler parameter ε.

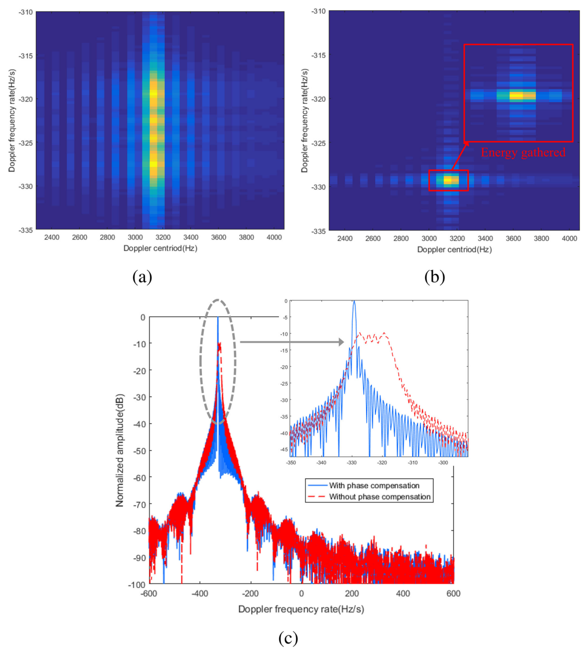

Fig. 4. The effect of the additional modulation term related to the third-order Doppler parameter ε. (a) 2D-FFT result without phase compensation. (b) 2D-FFT result with phase compensation. (c) The Doppler profiles of target signal after 2D-FFT.

It can be observed from (22) that the couplings between t-term, t^2-term, t^3-term and f_τ have been removed effectively and simultaneously. The RCMs of GMT with unknown curve motion have been well compensated. Meanwhile, the information of the Doppler parameters are still retained in GMT signal and the order of DFM is decreased after KDCT. The KDCT is put forward via multiplying the whole echo received in the corresponding aperture by its modified conjugation with a fixed delay in azimuth, which makes RCMC more efficient.

After performing KDCT, GMT signal has been gathered into a range cell. However, when GMT moves along a curve trajectory, the defocusing effect caused by the additional modulation term related to ε may not be neglected, especially with seconds long observation time. Consequently, signal in (22) can not be integrated via 2D-FFT, which leads to GMT energy smearing along the Doppler axis. Meanwhile, the broadening of signal will result in inaccurate Doppler parameter estimation, which is directly related to the performance of GMT refocusing. Thus, the estimation of ε and further compensation of the modulation term is necessary.

Then, FSFT is exploited to estimate the third-order Doppler parameter ε

$$\hat{\varepsilon} = -\lambda \times \arg\max_{\varepsilon} \left(FFT_t\left[S_3\left(t_\tau, t\right) \cdot H_{comp}\left(t_\tau, t, \varepsilon\right)\right]\right) \tag{23}$$

where $\hat{\varepsilon}$ is the estimation of ε. $FFT_t[\cdot]$ denotes the FFT operation with respect to t. $H_{comp}(f_\tau, t, \varepsilon)$ is constructed as

$$H_{comp}\left(f_\tau, t, \varepsilon\right) = \exp\left\{j\frac{\pi}{\lambda}\varepsilon t_0 t^2\right\} \tag{24}$$

Thus, the modulated phase compensation function is given by $H_{comp}(f_\tau, t, \hat{\varepsilon})$ according to (23). After performing modulation term compensation and azimuth FFT-range inverse FFT, the GMT signal in DC-DFR domain can be expressed as

$$S_4(f_{dc}, f_{dr}) = A\delta\left(f_{dc} + \frac{1}{\lambda}F_1\right)\delta\left(f_{dr} + F_2\right) \tag{25}$$

where A is the amplitude of the GMT signal in the DC-DFR domain. $\delta(\cdot)$ denotes the Dirac delta function. From (25), it can be seen that GMT signal with an unknown curve motion has been well integrated in DC-DFR domain.

Fig. 4 shows the effect of the additional modulation term related to the third-order Doppler parameter. Fig. 4(a) is the coherent integration result without the phase compensation in (24) and Fig. 4(b) is the result after the compensation. The Doppler profiles of target signal are given in Fig. 4(c). The red line represents the Doppler profile in Fig. 4(a). It can be seen that GMT signal after the 2D-FFT is still dispersed in multiple Doppler cells and its energy is not be completely accumulated. As a result, the performance on Doppler parameter estimation of the proposed method will be severely deteriorated due to the indetermination of the energy peak's position. The blue one represents the Doppler profile of GMT in Fig. 4(b). It obviously shows that GMT signal has been well accumulated into a peak after the phase compensation. And then, the estimation of the first- and second-order Doppler parameters can be easily obtained by resolving the peak's position.

Based on the peak detection technique, the DC and DFR of GMT can be simultaneously estimated. Through $(\hat{f}_{dc}, \hat{f}_{dr}) = \arg\max_{f_{dc}, f_{dr}}\{S_4(f_{dc}, f_{dr})\}$, we have

$$\hat{f}_{dc} = -\frac{1}{\lambda}F_1 = -\frac{1}{\lambda}\left(\frac{1}{2c}\alpha' t_0 + \frac{1}{12c}\varepsilon t_0^3\right) \tag{26}$$

$$\hat{f}_{dr} = -F_2 = -\left(\frac{\beta t_0}{\lambda} - \frac{1}{2\lambda}\varepsilon t_0^2\right) \tag{27}$$

Thus, substituting (23) into (26) and (27), the first- and second-order Doppler parameters can be obtained

$$\hat{\alpha} = \hat{\alpha}' - \lambda f_{ref} = -\frac{2c}{t_0}\lambda \hat{f}_{dc} - \frac{1}{6}\hat{\varepsilon} t_0^2 - \lambda f_{ref} \tag{28}$$

$$\hat{\beta} = \frac{1}{2}\hat{\varepsilon} t_0 - \frac{\lambda}{t_0}\hat{f}_{dr} \tag{29}$$

where $\hat{\alpha}$ and $\hat{\beta}$ are the estimations of α and β, respectively.

It is obvious from the (28)-(29) that both the estimated $\hat{\alpha}$ and $\hat{\beta}$ are determined by $\hat{\varepsilon}$ and t_0. In addition, the estimated accuracy of $\hat{\alpha}$ and $\hat{\beta}$ are determined by the range and Doppler resolution of system respectively.

By using the first- to third-order Doppler parameters estimated in (23), (28), and (29), the RCM and DFM in (13) can be accurately corrected. The RCM compensation function is given by

$$H_{RCM}(f_\tau, t) = \exp\left\{-j2\pi\frac{\lambda f_\tau}{c}\left(\hat{f}_{dc}t + \frac{1}{2}\hat{f}_{dr}t^2 + \frac{1}{6}\hat{f}_{d3}t^3\right)\right\} \tag{30}$$

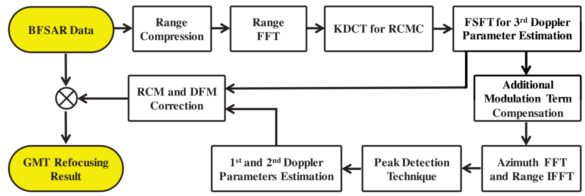

Fig. 5. The flowchart of the proposed KDCT-FSFT-based refocusing method.

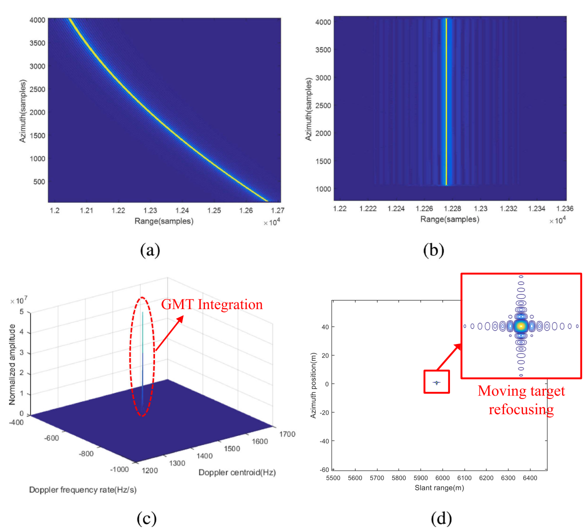

Fig. 6. Simulations results. (a) Range compression. (b) RCM correction. (c) 2D-FFT result. (d) GMT focusing on the estimated parameters.

where $\hat{f}_{dc}$, $\hat{f}_{dr}$, and $\hat{f}_{d3}$ are the estimated Doppler centroid, Doppler frequency rate and third-order Doppler frequency related to $\hat{\alpha}'$, $\hat{\beta}$ and $\hat{\varepsilon}$, respectively.

With the RCM correction, the DFM compression function can be obtained via the principle of stationary phase (POSP) [36], and it's given by

$$H_{DFM}(\tau, f_a) = \exp\left\{-j\frac{\pi\hat{f}_{d3}}{3\hat{f}_{dr}^3}f_a^3 + j\pi\left(\frac{1}{\hat{f}_{dr}}+\frac{\hat{f}_{d3}\hat{f}_{dc}}{\hat{f}_{dr}^3}\right)f_a^2\right\} \times \exp\left\{-\pi\left(\frac{2\hat{f}_{dc}}{\hat{f}_{dr}}+\frac{\hat{f}_{d3}\left(\hat{f}_{dc}\right)^2}{\hat{f}_{dr}^3}\right)f_a\right\} \quad (31)$$

Multiplying $H_{DFM}(\tau, f_a)$ by the RCM corrected signal in azimuth frequency domain and performing the azimuth inverse FFT (IFFT), GMT with unknown curve motion can be well refocused. The flowchart of the proposed method is shown in Fig. 5.

Compared with the methods in [24], [29], the proposed KDCT-FSFT can obtain a better refocusing performance, because the first- to third-order Doppler parameters can be estimated effectively. Additionally, since all the procedures in (21), (23) and (25) are performed with respect to all the range cells in the corresponding aperture, instead of every single range cell, which makes GMT refocusing in BFSAR more efficient and is highly desirable in practical applications.

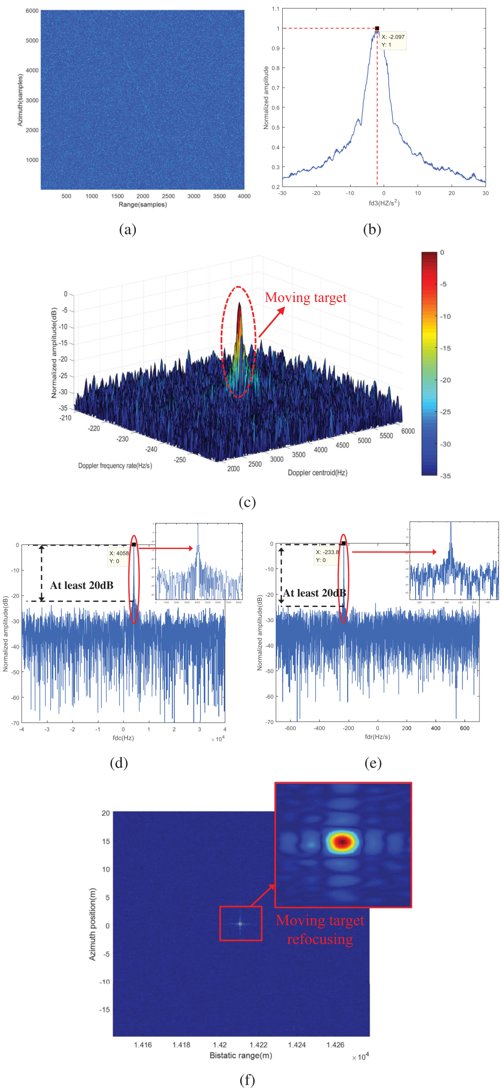

Fig. 7. Simulation with noise background. (a) Range compressed data. (b) Estimation of the third-order Doppler frequency. (c) Coherent integration. (d) Estimation of DC. (e) Estimation of DFR. (f) Refocused result of GMT.

Computational complexity analysis of Doppler parameters estimation: Assuming that N, M and N_p denote the number of range cells, azimuth pulses and searching times of the Doppler parameters, respectively. Generally, N_p is much larger than N and M. For the proposed method, its major implementation procedures include the pre-filtering (MN), KDCT for the range cell migration correction $((M+1)MN + 0.5NM\log_2^N)$, FSFT for the third-order Doppler parameter estimation $(N_p(0.5NM\log_2^M + MN))$ and 2D-FFT $(0.5NM\log_2^N + 0.5NM\log_2^M)$. Thus, the total computational cost is

$$F_p = (M+2)MN + N_p(MN + 0.5MN\log_2^M) + MN\log_2^N + 0.5MN\log_2^M \quad (32)$$

Let $M = N = N_p$, the computational complexity of the proposed method is on the order of $O(N^3\log_2^N)$.

TABLE II
BFSAR SYSTEM PARAMETERS

Parameters	Values
Center frequency	$10GHz$
Range bandwidth	$300MHz$
Pulse repetition frequency	$1500Hz$
Platform velocity	$150m/s$
Transmitter's location	$(-3000, -2000, 6000)m$
Receiver's location	$(0, -4000, 6000)m$

TABLE III
ESTIMATION RESULT OF THE PROPOSED METHOD

	Doppler frequency related to $\hat{\alpha}$, $\hat{\beta}$ and $\hat{\varepsilon}$		
	$f_{dc}(Hz)$	$f_{dr}(Hz/s)$	$f_{d3}(Hz/s^2)$
True value	4058.2062	-233.8186	-2.1028
Estimated value	4057.9495	-233.7985	-2.0970
Estimated error	-0.2567	0.0201	0.0058

TABLE IV
FOCUSING PERFORMANCE

	Resolution(m)	PSLR(dB)	ISLR(dB)
Azimuth	0.2964	-13.07	-10.2033
Range	0.8889	-12.86	-10.0374

PLSR:peak sidelobe ratio; ISLR:integrated sidelobe ratio.

TABLE V
RELEVANT PARAMETERS

Parameters	Values
Center frequency	$10GHz$
Range bandwidth	$300MHz$
Pulse repetition frequency	$1000Hz$
Transmitter's location	$(-1000, -400, 800)m$
Receiver's location	$(0, -1200, 800)m$

IV. SIMULATION RESULTS

To verify the effectiveness of the proposed BFSAR GMT refocusing method based on KDCT-FSFT, simulations are carried out in this section. In the following, a noise-free example is given to evaluate the proposed method as depicted in Fig. 6, where the system parameters are set as: $f_c = 10$ GHz, $B_\tau = 300$ MHz, $T_a = 2$ s, $V_R = V_T = 160$ m/s and pulse repetition frequency (PRF) is 1500 Hz. The original coordinates of receiver and transmitter are (0, -1000, 3500) m and (-1200, 0, 2000) m respectively. A GMT moving along a curve trajectory is considered. The velocity vector of GMT is set as (3 m/s, -4m/s; 2 m/s^2, -2m/s^2) and GMT is located at the scene center at the beam center crossing time. After range compression, it can be seen that GMT signal is dispersed into multiple range cells in Fig. 6(a). Fig. 6(b) is the result of RCMC after KDCT, it obviously shows that GMT has been gathered into one range cell without any Doppler information of the GMT. Fig. 6(c) is the 2D-FFT result of GMT in DC-DFR domain after FSFT, and one can see that GMT has been well integrated in DC-DFR domain. According to FSFT and the peak's position in Fig. 6(c), the Doppler parameters of GMT can be obtained effectively.

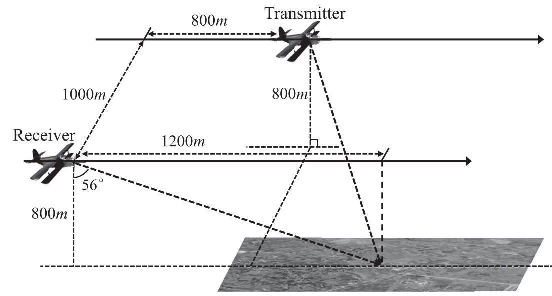

Fig. 8. Geometry configuration in airborne BFSAR experiment.

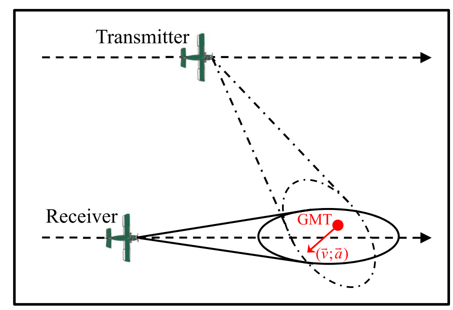

Fig. 9. The top view of geometry relationship between platforms and GMT.

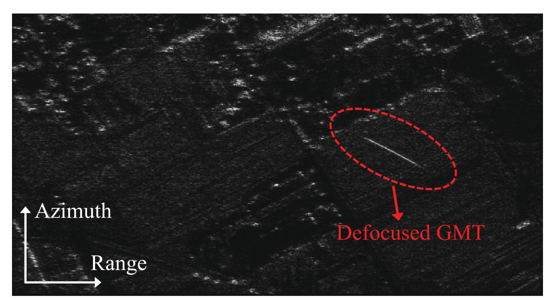

Fig. 10. Imaging result of the stationary scene without processing of GMT.

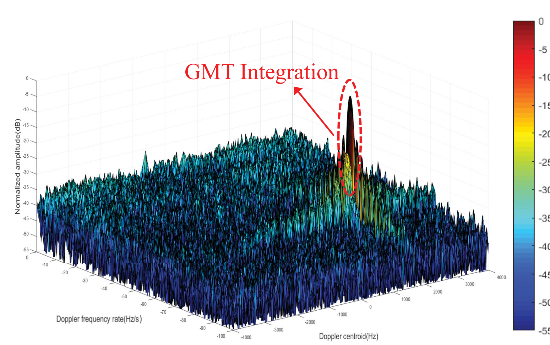

Fig. 11. Coherent integration in DC-DFR domain.

Finally, GMT signal in (13) can be finely refocused with the estimated Doppler parameters, as depicted in Fig. 6(d).

To further analyze the performance of the proposed method, simulation with a noise background is given in Fig. 7. The BFSAR system parameters are given in Table II. The velocity vector of GMT is set as (10 m/s, -6 m/s; 2 m/s^2, 1 m/s^2).

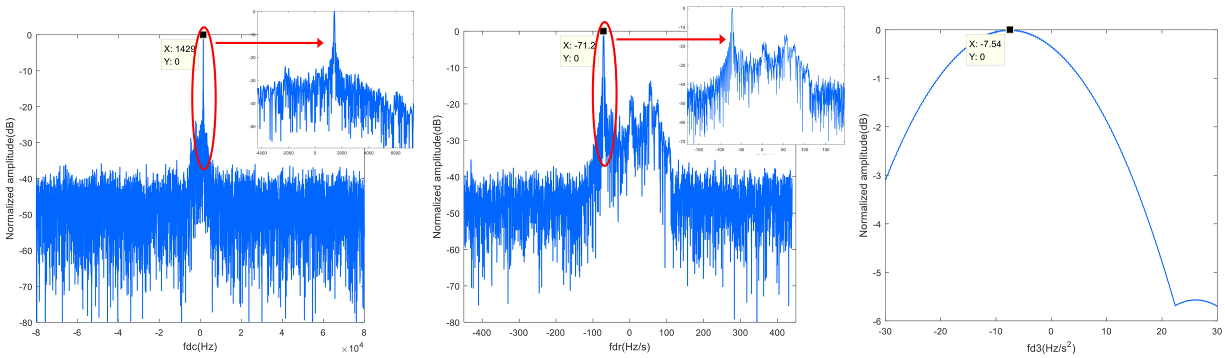

(a) (b) (c)

Fig. 12. Estimated results of the Doppler parameters. (a) Doppler centroid. (b) Doppler frequency rate. (c) The third-order Doppler frequency.

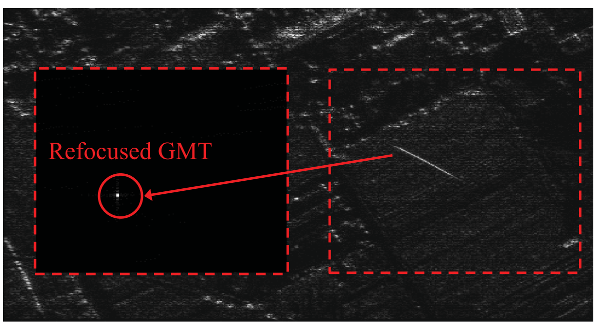

Fig. 13. The refocused result of the GMT.

Assuming that GMT is dim small, and the SNR is set to be -35 dB. Fig. 7(a) is the range compressed result of BFSAR echo. It can be seen that GMT is buried in background noise after range compression, since GMT signal is dispersed in multiple cells caused by RCM and DFM. After the RCM compensation, the third-order parameter can be estimated by FSFT and the phase compensation can be performed. Fig. 7(b) is the estimated result of f_{d3}. With the proposed method, GMT can be well coherent integrated in DC-DFR domain, as depicted in Fig. 7(c). The color scale is in dB, where 0 dB denotes the maximum intensity. From this figure, one can see that SNR has been greatly improved and GMT can be easily detected by the peak detection. Then, the first- and second-order Doppler parameters of GMT can be estimated by resolving the position of the peak. The estimated results are shown in Fig. 7(d) and Fig. 7(e), where the SNR has been improved at least 20 dB. Fig. 7(f) presents refocused result of GMT.

According to (7)–(9) and the simulation results presented above, the comparison between the Doppler frequency calculated by the estimated Doppler parameters and the true values is given in Table III. The estimated errors of f_{dc}, f_{dr}, and f_{d3} are -0.2567 Hz, 0.0201 Hz/s and 0.0058 Hz/s^2, respectively. Compared with the true values, the impact of these errors on GMT refocusing can be neglected. The first-, second- and third-order Doppler parameters are efficiently and accurately estimated by the proposed method. In addition, the refocusing performance of GMT is shown in Table IV. The azimuth and range resolution of the BFSAR system are 0.2964 and $0.8889m$, respectively. The theoretical range resolution is $0.886(c/B_\tau) = 0.886m$ and the theoretical azimuth resolution is $0.886(V_R/B_a) = 0.2842m$, where B_a is the azimuth frequency bandwidth. It can be seen that the measured range resolution of GMT by the proposed method is agree well with the theoretical value. The azimuth resolution has a maximum broadening of about 4.3%. The theoretical values of the peak sidelobe ratio (PSLR) and integrated sidelobe ratio (ISLR) are -13.27 and -10.24 dB. For the proposed method, the range and azimuth PSLR values have a less than 0.45 dB from the theoretical values. As for ISLR, the measured results have a deviation less than 0.2 dB from the theoretical value.

V. Experimental Results

In this section, the effectiveness of the proposed method will be demonstrated by the X-band BFSAR data, combined with simulated GMT signal. That is, the stationary background echo are real data and GMT data are injected by simulation. The X-band BFSAR data are recorded by two airplanes in the experiment in Chengdu, 2016. In this experiment, the velocity of the transmitter and receiver were 40 m/s. The flight heights of platforms were $800m$. The other specific parameters of this BFSAR system are listed in Table V. Fig. 8 shows the geometry configuration.

A GMT with curve motion is considered and its velocity is $(v_x, v_y) = (4, -3)$ m/s. The cross-track acceleration and along-track acceleration of GMT are set as $(a_x, a_y) = (2, -1)$ m/s^2. The original coordinate of GMT is (80, 0, 0) m. In the experiment, the transmitter and receiver were flying parallelly with the same velocity 40 m/s. According to the theoretical calculation, the equivalent Doppler frequency of GMT can be calculated as: $f_{dc} = 1429.975$ Hz, $f_{dr} = -71.152$ Hz/s, $f_{d3} = -7.758$ Hz/s^2. The signal to clutter and noise ratio (SCNR) of GMT is set to be -15 dB. The top view of geometrical relationship between platforms and GMT is shown in Fig. 9.

Fig. 10 is the imaging result without the processing of GMT. Due to the mismatch between the GMT's RCM and Doppler parameters with those of background, GMT is smearing along range and azimuth axis, which has been highlighted by red dotted

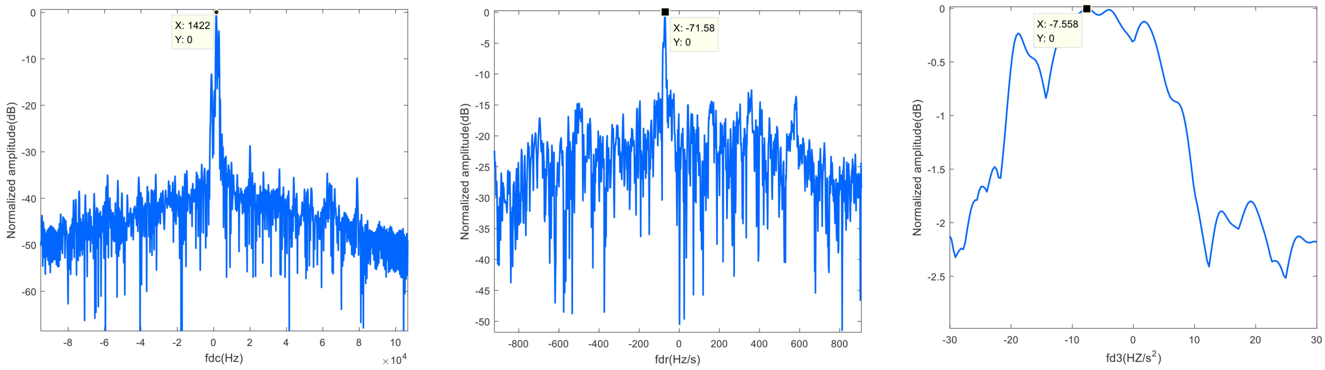

(a) (b) (c)

Fig. 14. Estimation results of the distributed GMT. (a) Doppler centroid. (b) Doppler frequency rate. (c) The third-order Doppler frequency.

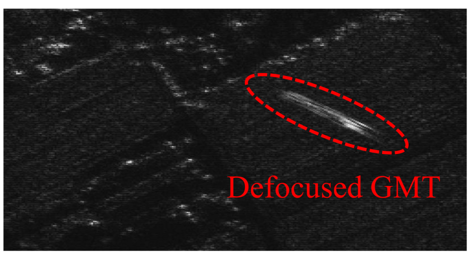

(a)

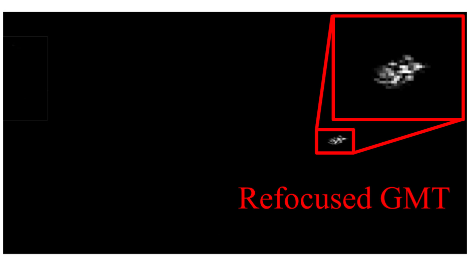

(b)

Fig. 15. Simulation results with the distributed GMT. (a) Image with defocused distributed GMT. (b) Refocused distributed GMT.

circles. And then, the coherent integration result of GMT in DC-DFR domain is shown in Fig. 11. It clearly shows that GMT has been well accumulated into a peak and it can be easily detected by peak detection technique in the integration domain.

Fig. 12 shows the profiles of GMT's integrated peak. By resolving peak's position in (26) and (27), Doppler parameters of GMT can be estimated. Based on the estimated $\hat{\alpha}$, $\hat{\beta}$ and $\hat{\varepsilon}$, Doppler frequency can be obtained as: f_{dc} =1428.553 Hz, $f_{dr} = -71.204$ Hz/s, $f_{d3} = -7.540$ Hz/s^2. The estimation results are almost in accordance with the theoretical values (f_{dc} =1429.975 Hz, $f_{dr} = -71.152$ Hz/s, $f_{d3} = -7.758$ Hz/s^2). The estimated errors of f_{dc}, f_{dr}, and f_{d3} are -1.422 Hz, -0.052 Hz/s, and 0.218 Hz/s^2, respectively. The corresponding estimated errors are less than 0.10%, 0.07%, 2.81% from the theoretical values, respectively, which can be ignored for GMT refocusing. The Doppler parameters of GMT with unknown curve motion have been accurately estimated. With the estimated Doppler parameters, RCM and DFM of GMT can well compensated by (30)–(31). The refocused result of GMT is presented in Fig. 13. It can be seen that GMT can be well refocused in the image with the proposed KDCT-FSFT-based refocusing method.

To further verify the validity of the proposed method, simulation with a distributed target is performed in the following. The simulated target is a distributed GMT in a real data SAR image. During the simulation, the motion parameters of the distributed GMT are set similar with those in pointlike GMT simulations given above. With the proposed method, the Doppler frequencies of the distributed GMT can be estimated as: f_{dc} =1422.24 Hz, $f_{dr} = -71.58$ Hz/s, and $f_{d3} = -7.56$ Hz/s^2 (shown in Fig. 14), and the estimated errors are less than 0.54%, 0.61% and 2.57% from the theoretical values in this case. Fig. 15 shows the imaging result without processing of GMT and the refocused result via KDCT-FSFT. From Fig. 15(b), we can observe that the distributed GMT with a varied backscattering characteristic has been refocused by the proposed method.

VI. Conclusion

In this article, we have proposed a KDCT-FSFT-based refocusing method for GMT with unknown curve motion in BFSAR cases. The contributions of the proposed method include the following: 1) the range walk, range curvature and third-order RCM caused by GMT's curve movement can be effectively and simultaneously corrected by KDCT without any priori motion information. Meanwhile, the order of DFM can be reduced as well in KDCT. 2) the proposed method is easy to be implemented by complex multiplications and FFTs, and it has a good performance on GMT refocusing, since the first- to third-order Doppler parameters of GMT can be estimated accurately. 3) Refocused processing for GMT with unknown curve motion is going with the BFSAR echo data of all the range cells in the corresponding aperture, which make the proposed method more efficient and practical in realistic applications. The effectiveness of the method has been validated by simulation and experimental results.

REFERENCES

[1] J. Wu, J. Yang, Y. Huang, H. Yang, and H. Wang, "Bistatic forward-looking SAR: Theory and challenges," in *Proc. IEEE Radar Conf.*, Pasadena, CA, 2009, pp. 1–4.

[2] R. Wang, O. Loffeld, H. Nies and V. Peters, "Image formation algorithm for bistatic forward-looking SAR," in *Proc. IEEE Int. Geosci. Remote Sens. Symp.*, Honolulu, HI, 2010, pp. 4091–4094.

[3] I. Walterscheid, T. Espeter, J. Klare, A. R. Brenner and J. H. G. Ender, "Potential and limitations of forward-looking bistatic SAR," in *Proc. IEEE Int. Geosci. Remote Sens. Symp.*, Honolulu, HI, 2010, pp. 216–219.

[4] J. Yang *et al.*, "A first experiment of airborne bistatic forward-looking SAR - Preliminary results," in *Proc. IEEE Int. Geosci. Remote Sens. Symp.*, Melbourne, VIC, 2013, pp. 4202–4204.

[5] T. Espeter, I. Walterscheid, J. Klare, A. R. Brenner, and J. H. G. Ender, "Bistatic Forward-Looking SAR: Results of a Spaceborne–CAirborne experiment," in *Proc. IEEE Geosci. Remote Sens. Lett.*, vol. 8, no. 4, pp. 765–768, Jul. 2011.

[6] S. Suchandt and H. Runge, "Ocean surface observations using the TanDEM-X satellite formation," *IEEE J.Sel. Topics Appl. Earth Observ. Remote Sens.*, vol. 8, no. 11, pp. 5096–5105, Nov. 2015.

[7] S. V. Baumgartner and G. Krieger, "Simultaneous High-Resolution Wide-Swath SAR imaging and ground moving target indication: Processing approaches and system concepts," *IEEE J.Sel. Topics Appl. Earth Observ. Remote Sens.*, vol. 8, no. 11, pp. 5015–5029, Nov. 2015.

[8] J. Yang, C. Liu and Y. Wang, "Detection and imaging of ground moving targets with real SAR data," *IEEE Trans. Geosci. Remote Sens.*, vol. 53, no. 2, pp. 920–932, Feb. 2015.

[9] X. Li, M. Xing, X. Xia, G. Sun, Y. Liang, and Z. Bao, "Simultaneous stationary scene imaging and ground moving target indication for High-Resolution Wide-Swath SAR system," *IEEE Trans. Geosci. Remote Sens.*, vol. 54, no. 7, pp. 4224–4239, Jul. 2016.

[10] Z. Li, S. Li, Z. Liu, H. Yang, J. Wu, and J. Yang, "Bistatic Forward-Looking SAR MP-DPCA method for Space-Time extension clutter suppression," *IEEE Trans. Geosci. Remote Sens.*, Mar. 2020.

[11] P. Lombardo, D. Pastina and F. Turin, "Ground moving target detection based on MIMO SAR systems," *IEEE J.Sel. Topics Appl. Earth Observ. Remote Sens.*, vol. 8, no. 11, pp. 5081–5095, Nov. 2015.

[12] P. Huang, X. Zhang, Z. Zou, X. Liu, G. Liao, and H. Fan, "Road-Aided Along-Track baseline estimation in a multichannel SAR-GMTI system," *IEEE Geosci. Remote Sens. Lett.*, 2020.

[13] P. Huang, J. Ma, H. Xu, X. Liu, X. Jiang, and G. Liao, "Moving target focusing in SAR imagery based on subaperture processing and DART," *IEEE Geosci. Remote Sens. Lett.*, 2020.

[14] P. Huang, X. Xia, Y. Gao, X. Liu, G. Liao, and X. Jiang, "Ground moving target refocusing in SAR imagery based on RFRT-FrFT," *IEEE Trans. Geosci. Remote Sens.*, vol. 57, no. 8, pp. 5476–5492, Aug. 2019.

[15] J. Zheng, T. Yang, H. Liu, and T. Su, "Efficient Data Transmission Strategy for IIoTs with Arbitrary Geometrical Array," *IEEE Trans. Ind. Inform.*, 2020.

[16] J. Zheng, H. Liu, and Q. H. Liu, "Parameterized centroid frequency-chirp rate distribution for LFM signal analysis and mechanisms of constant delay introduction," *IEEE Trans. Signal Process.*, vol. 65, no. 24, pp. 6435–6447, 2017.

[17] Z. Li, J. Wu, Z. Liu, Y. Huang, H. Yang, and J. Yang, "An Optimal 2-D Spectrum Matching Method for SAR Ground Moving Target Imaging," *IEEE Trans. Geoscie. Remote Sens.*, vol. 56, no. 10, pp. 5961–5974, Oct. 2018.

[18] C. Wu, K. Liu, and M. Jin, "A modeling and corrrelation algorithm for Spaceborne SAR signals," *IEEE Trans. Aerosp. Electron. Syst.*, vol. AES-18, no. 5, pp. 563–574, Sep. 1982.

[19] G. Davidson, I. Cumming and M. Ito, "A chirp scaling approach for processing squint mode SAR data," *IEEE Trans. Aerosp. Electron. Syst.*, vol. 32, no. 1, pp. 121–133, Jan. 1996.

[20] H. Shin and J. Lim, "Omega-k Algorithm for Airborne Forward-Looking Bistatic Spotlight SAR Imaging," *IEEE Geosci.Remote Sens. Lett.*, vol. 6, no. 2, pp. 312–316, Apr. 2009.

[21] H. Xie, S. Shi, D. An, G. X. Wang, G. Q. Wang and H. Xiao, "Fast Factorized Backprojection Algorithm for One-Stationary Bistatic Spotlight Circular SAR Image Formation," *IEEE J. Sel. Topics Appl. Earth Observ. Remote Sens.*, vol. 10, no. 4, pp. 1494–1510, Apr. 2017.

[22] Y. Li, P. Huang, Z. Yang, and C. Lin, "Parameter estimation and imaging of moving targets in bistatic synthetic aperture radar," *J. Appl. Remote Sens.*, vol. 10, no. 1, Art. no. 015018, 2016.

[23] B. Zhu, Z. Tang, Y. Zhang, and X. Jiang, "The estimation of Doppler parameter of bistatic SAR based on radon translation," *J.Electron. Inform. Technol.*, vol. 30, no. 6, pp. 1331–1335, 2008.

[24] Z. Li, J. Wu, Q. Yi, Y. Huang, J. Yang and Y. Bao, "Bistatic forward-looking SAR ground moving target detection and imaging," *IEEE Trans. Aerosp. Electron. Syst.*, vol. 51, no. 2, pp. 1000–1016, Apr. 2015.

[25] S. Yuan, T. Wu, M. Mao, G. Mei and X. Wei, "Application research of keystone transform in weak high-speed target detection in low-PRF narrowband Chirp radar," in *Proc. 2008 9th Int. Conf. Signal Process.*, Beijing, 2008, pp. 2452–2456.

[26] D. Zhu, Y. Li and Z. Zhu, "A keystone transform without interpolation for SAR ground moving-target imaging," *IEEE Geosci. Remote Sens. Lett.*, vol. 4, no. 1, pp. 18–22, Jan. 2007.

[27] Z. Sun, J. Wu, Y. Huang, Z. Li, H. Yang and J. Yang, "Ground moving target detection in squint SAR imagery based on extended Azimuth NLCS and Deramp processing," in *Proc. IEEE Int. Geosci. Remote Sens. Symp.*, Quebec City, QC, 2014, pp. 600–603.

[28] R. Wang *et al.*, "Focusing bistatic SAR data in airborne/stationary configuration," *IEEE Trans. Geosci. Remote Sens.*, vol. 48, no. 1, pp. 452–465, Jan. 2010.

[29] Z. Li, J. Wu, Y. Huang, Z. Sun and J. Yang, "Ground-moving target imaging and velocity estimation based on mismatched compression for bistatic forward-looking SAR," *IEEE Trans. Geosci. Remote Sens.*, vol. 54, no. 6, pp. 3277–3291, Jun. 2016.

[30] P. V. C. Hough, "Method and means for recognizing complex patterns," U.S. Patent 3 069 654, Dec. 18, 1962.

[31] F. Zhou, R. Wu, M. Xing and Z. Bao, "Approach for single channel SAR ground moving target imaging and motion parameter estimation," *IET Radar, Sonar Navigation*, vol. 1, no. 1, pp. 59–66, Feb. 2007.

[32] C. Huang, Z. Li, J. Wu, Y. Huang, H. Yang, and J. Yang, "Multistatic Beidou-based passice radar for maritime moving target detection and localization," in *Proc. IEEE Int. Geosci. Remote Sens. Symp.*, Yokohama, Japan, 2019.

[33] P. Huang, X. Xia, G. Liao and Z. Yang, "Ground moving target imaging based on keystone transform and coherently integrated CPF with a single-channel SAR," *IEEE J. Sel. Topics Appl. Earth Observ. Remote Sens.*, vol. 10, no. 12, pp. 5686–5694, Dec. 2017.

[34] Y. Lan, Z. Li, J. Qu, J. Wu and J. Yang, "A fast doppler parameters estimation method for moving target imaging based on 2D-FFT," in *Proc. IEEE Int. Geosci. Remote Sens. Symp.*, Valencia, 2018, pp. 589–592

[35] S. Peleg and F. Benjamin, "The discrete polynomial-phase transform," *IEEE Trans. Signal Process.*, vol. 43, no. 8, pp. 1901–C1914, Aug. 1995.

[36] I. G. Cumming and F. H. Wong, *Digit. Process. Synthetic Aperture Radar Data: Algorithms and Implementation.* Norwood, MA, USA: Artech House, 2005.

[37] J. Yang and Y. Zhang, "An airborne SAR moving target imaging and motion parameters estimation algorithm with azimuth-dechirping and the second-order keystone transform applied," *IEEE J. Sel. Topics Appl. Earth Observ. Remote Sens.*, vol. 8, no. 8, pp. 3967–3976, Aug. 2015.